12th International Symposium on Turbulence and Shear Flow Phenomena (TSFP12)
Osaka, Japan, July 19–22, 2022

LOGARITHMIC SCALING OF HIGHER-ORDER TEMPERATURE MOMENTS IN THE ATMOSPHERIC SURFACE LAYER

Kelly Y. Huang
Dept of Civil and Environmental Engineering
University of Notre Dame
Notre Dame, IN, 46556, United States
yhuang28@nd.edu

Matt K. Fu
GALCIT
Caltech
Pasadena, CA 91125, USA
mkfu@caltech.edu

Clayton P. Byers
Dept of Engineering
Trinity College
Hartford, CT, 06106, United States
clayton.byers@trincoll.edu

Gabriel G. Katul
Dept of Civil and Environmental Engineering
Duke University
Durham, NC, 27708, United States
gaby@duke.edu

ABSTRACT

A generalized logarithmic law for high-order moments of passive scalars is proposed. This law is analogous to the generalized log law that has been proposed for high-order moments of the turbulent longitudinal velocity and is derived by combining the random sweeping decorrelation hypothesis with a spectral model informed by the attached eddy hypothesis. The proposed theory predicts that the high-order moments of passive scalar fluctuations within the inertial sublayer will vary logarithmically with distance from a boundary (z). The proposed theory is evaluated using highly resolved time-series measurements of temperature and streamwise velocity fluctuations obtained in the first meter of the atmospheric surface layer (ASL) under near-neutral thermal stratification. The logarithmic dependence with z within the inertial sublayer is observed in both the air temperature and velocity moments, with good agreement to the predictions from the proposed theory. Surprisingly, the proposed theory appears to be as, if not more, valid for transported passive scalars than for the longitudinal velocity.

BACKGROUND

A stationary and planar-homogeneous turbulent boundary layer flow at high Reynolds number (Re) is considered here with w', u' and θ_v' defining the wall-normal velocity, streamwise velocity, and virtual potential temperature fluctuations, respectively, and primed quantities are turbulent fluctuations from the mean state that is indicated by overline. These assumptions ensure that the friction velocity $u_* = \sqrt{-\overline{u'w'}}$ and the temperature scale $\theta_* = -\overline{w'\theta'}/u_*$ are independent of distance z from the boundary.

The random sweeping decorrelation hypothesis (RSDH) is a kinematic model predicated on the assumption that small-scale eddies are swept by the larger, energetic eddies without any dynamic distortion (Tennekes, 1975). Hence, motion of the smaller scales, particularly in the inertial range, are due to the kinetic energy of the large scales. A consequence of this kinematic assumption is the tendency towards Gaussian behavior, which has known analytical expressions for the probability distribution function and subsequent statistics.

By assuming a Gaussian distribution for u' and that the eddies are non-interacting, Meneveau & Marusic (2013) were able to develop a generalized logarithmic-law relation for the high-order statistics of u' in the inertial sublayer given by

$$\left(\overline{u'^{2p}}^{+}\right)^{1/p} = B_p - A_p \ln\left(\frac{z}{\delta}\right), \tag{1}$$

where $p \geq 1$ is the moment order, B_p is a flow-dependent constant, $A_p = A_1\left[(2p-1)!!\right]^{1/p}$, $A_1 \approx 1.25$ is the Townsend-Perry constant (see Smits *et al.*, 2011; Marusic *et al.*, 2013; Meneveau & Marusic, 2013), !! is the double factorial, z is the wall-normal distance, δ is an outer length scale such as the boundary layer height, and the $+$ superscript indicates normalization by the friction velocity u_*. The scaling law of equation 1 was recovered through simpler arguments that take advantage of (i) RSDH to generalize the behavior of high-order spectra and (ii) the consequences of the attached eddy model on the conventional spectrum of u' (Katul *et al.*, 2016). In arriving at equation 1, high-order spectra were related via RSDH to a model spectrum for u' characterized by a k^{-1} scaling regime of wavenumber k at large scales (i.e. attached eddies) and $k^{-5/3}$ for inertial scales (i.e. detached eddies) up to the Kolmogorov micro-scale. Integration of this model spectrum and its combination with RSDH then recovered equation 1 and linked A_p and B_p explicitly to the Kolmogorov constant and Re for Gaussian statistics. While RSDH has been investigated extensively in terms of the turbulent velocity, particularly u', significantly less attention has been paid to the behavior of passive scalars such as temperature in near-neutral stratification. Previous numerical studies have indicated that in isotropic turbulence, passive scalar fields adhere to the RSDH as well as, if not better than, the velocity field (Yeung & Sawford, 2002).

Here, a new theory is proposed based on RSDH and the similarity between temperature and streamwise momentum for the behavior of passive scalar moments in the inertial sublayer. Following the methodology of Huang & Katul (2022), we de-

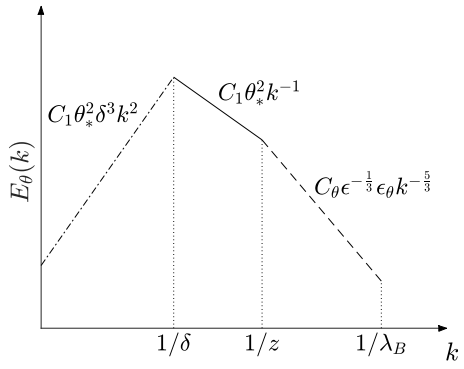

Figure 1. Illustration of an idealized piece-wise temperature spectrum and its scaling regimes as a function of wavenumber k. The k^2 behavior (analogous to the Saffman spectrum) is the minimum required for $dE_\theta/dk \to 0$ as $k \to 0$. For analytical tractability, the Kolmogorov $k^{-5/3}$ inertial scaling is extended to the Batchelor scale with a cutoff compensating for the energy contribution not resolved here by the expected exponential decay due to molecular effects.

rive an analogous logarithmic law for the high-order statistics of temperature fluctuations $\overline{\theta'^{2p}}$ by combining the predictions of RSDH with those from the attached eddy hypothesis in near neutral stability conditions. The predicted behavior is found to be in agreement with highly resolved measurements of temperature obtained in the atmospheric surface layer under near-neutral conditions. Further, the deviations between the temperature statistics and their corresponding theoretical predictions are found to be significantly smaller than those found for the collocated streamwise velocity.

THEORY

Direct numerical simulations of a turbulent channel up to $Re_\tau \leq 4088$ for $Pr = 0.7-1$ revealed qualitative agreement between the streamwise velocity variance and passive scalar variance (Pirozzoli *et al.*, 2016). Additionally, a k^{-1} scaling of temperature spectra in the atmospheric surface layer has been found with good agreement in multiple stability conditions (Pond *et al.*, 1966; Katul *et al.*, 1995; Li *et al.*, 2016) and the current measurements here. Combining these results with Katul *et al.* (2016) and Huang & Katul (2022) allows for the theoretical development of a logarithmic law in the high-order even moments of the temperature variance given by

$$\left(\overline{\theta'^{2p}}^{+}\right)^{1/p} = B_{p,\theta} - A_{p,\theta}\ln\left(\frac{z}{\delta}\right), \tag{2}$$

where $B_{p,\theta}$ is a flow-dependent offset, $A_{p,\theta}$ is the slope, analogous to the Townsend-Perry constant in equation 1, and the $+$ superscript again indicates normalization by the friction velocity and scalar wall flux.

For a θ' time series, the integral of the p^{th} order spectrum, $E_\theta^{(p)}(k)$, is related to statistical moments of θ' through

$$\overline{(\theta'^p - \overline{\theta'^p})^2} = \overline{\theta'^{2p}} - \overline{\theta'^p}^2 = \int_0^{+\infty} E_\theta^{(p)}(k)\,dk. \tag{3}$$

Under the assumptions of RSDH, the probability distribution function (PDF) of the time series will be normally distributed, allowing the higher order statistical moments and spectra to be expressed as a function of the second ($p = 1$) moment resulting in

$$E_\theta^{(p)}(k) = \alpha(p)\overline{\theta'^2}^{p-1}E_\theta(k), \tag{4}$$

where $\alpha(p) = p^2 \times 1 \times 3 \times 5 \times \ldots \times (2p-3)$ is a consequence of Gaussian statistics for $p > 1$.

The high-order moments for temperature $\overline{\theta'^{2p}} = \int_0^\infty E_\theta^{(p)}(k)\,dk + \overline{\theta'^p}^2$ are now interpreted with the RSDH (see equation 4) to yield

$$\overline{\theta'^{2p}} = \alpha(p)\left[\overline{\theta'^2}\right]^{p-1}\int_0^\infty E_\theta(k)\,dk + \overline{\theta'^p}^2. \tag{5}$$

It can be shown for Gaussian statistics that the $\overline{\theta'^p}^2$ term is zero for odd p and diminishes rapidly for even p so that its contribution is only significant for $p = 2$ with a value of $(3/2)\overline{\theta'^{2p}}$.

To arrive at an analytic expression, an idealized shape for $E_\theta(k)$ is prescribed and shown in figure 1 based on Huang & Katul (2022) and given by the piecewise function

$$E_\theta(k) = \begin{cases} C_1\theta_*^2\delta^3k^2 & \text{if } k \in [0, \delta^{-1}] \\ C_1\theta_*^2k^{-1} & \text{if } k \in [\delta^{-1}, z^{-1}] \\ C_\theta\overline{\varepsilon_\theta}^{-2/3}k^{-5/3} & \text{if } k \in [z^{-1}, \lambda_B^{-1}] \\ 0 & \text{if } k > \lambda_B^{-1}, \end{cases} \tag{6}$$

where $\lambda_B = Sc_m^{-1/2}\eta$ is the Batchelor scale, close to the Kolmogorov microscale η in near-neutral atmospheric flows because the molecular Schmidt number (Sc_m) is close to unity for temperature and many other scalars. Assuming that production of turbulent kinetic energy and temperature variance are each balanced by their respective dissipation within the inertial sublayer (i.e., $\varepsilon = u_*^3/\kappa z$ and $\varepsilon_\theta = u_*\theta_*^2/\kappa z$, and $\kappa \approx 0.41$), the spectral model in equation 6 can be integrated, giving

$$\int_0^\infty E_\theta(k)\,dk = \overline{\theta'^2} = \int_0^{1/\delta} C_1\theta_*^2\delta^3k^2\,dk + \int_{1/\delta}^{1/z} C_1\theta_*^2k^{-1}\,dk + \int_{1/z}^{1/\lambda_B} C_\theta\overline{\varepsilon_\theta}^{-2/3}k^{-5/3}\,dk,$$

and allowing the temperature variance to ultimately be expressed as

$$\frac{\overline{\theta'^2}}{\theta_*^2} \equiv \overline{\theta'^2}^{+} = C_1\left[\frac{11}{6} - \frac{3}{2}\left(\frac{\lambda_B}{z}\right)^{2/3}\right] - C_1\ln\left(\frac{z}{\delta}\right), \tag{7}$$

so that $A_{1,\theta} = C_1$ and $B_{1,\theta} = C_1\left[\frac{11}{6} - \frac{3}{2}\left(\frac{\lambda_B}{z}\right)^{2/3}\right]$. Note the value of C_θ is related to C_1 through matching the piecewise function at $k = 1/z$. Equation 5 can then be written as

$$\overline{\theta'^{2p}} = \alpha(p)\left[\overline{\theta'^2}\right]^{p-1}\theta_*^2\left[B_{1,\theta} - A_{1,\theta}\ln\left(\frac{z}{\delta}\right)\right]. \tag{8}$$

Finally, substituting $\overline{\theta'^2} = \theta_*^2\left[B_{1,\theta} - A_{1,\theta}\ln\left(\frac{z}{\delta}\right)\right]$, normalizing by θ_*^{2p}, and raising to a power of $1/p$ provides the sought

result

$$(\overline{\theta'^{2p}}^{+})^{1/p} = \alpha(p)^{1/p}\left[B_{1,\theta} - A_{1,\theta}\ln\left(\frac{z}{\delta}\right)\right]. \quad (9)$$

This expression has the same form as equation 2 with $A_{p,\theta} = \alpha(p)^{1/p}A_{1,\theta}$ and $B_{p,\theta} = \alpha(p)^{1/p}B_{1,\theta}$.

EXPERIMENTAL METHODOLOGY & DATA

As part of the Idealized horizontal Planar Array study for Quantifying Surface heterogeneity (IPAQS) (Morrison *et al.*, 2021) that took place at the Surface Layer Turbulence and Environmental Science Test (SLTEST) facility in the western deserts of Utah, USA, measurements of longitudinal velocity and temperature were acquired at z = 0.0625, 0.125, 0.25, 0.5, and 1.0 m above the ground during a three-day intensive sampling period (18 - 20 June 2018). The SLTEST facility is a unique field site with near-canonical boundary conditions (its aerodynamic roughness ranges from sub-millimeter to less than 6 mm) and predictable wind patterns, making it an ideal location for probing high *Re* turbulent boundary layer flows (Klewicki *et al.*, 1998; Metzger & Klewicki, 2001). The equivalent sand grain roughness for these measurements was estimated to be 2.5 mm using the relation for a zero-pressure-gradient neutral boundary layer (Huang *et al.*, 2021*a*), meaning lowest station height corresponds to 25 times that of the equivalent sand grain roughness.

Nano-scale thermal anemometry probes (NSTAPs) operated in constant-current anemometry mode and their cold-wire variants (TNSTAPs) were used to capture velocity and temperature measurements, respectively, at each height with a sampling frequency of 100 Hz. The sensing elements of these nano-scale sensors are platinum wire ribbons 2 μm in width, 100 nm in thickness, 60 μm in length for the NSTAP and 200 μm in length for the TNSTAP. The size of these sensors provide high spatial resolution with minimized end-conduction effects and temporal filtering (Hultmark *et al.*, 2011; Arwatz *et al.*, 2015). Relevant stresses and heat fluxes are calculated from data taken by a nearby triaxial sonic anemometer (Campbell Scientific CSAT3) at approximately 10 m west of the measurement tower at $z = 2$ m. Further details regarding the experimental set-up and calibration procedure can be found elsewhere (Huang *et al.*, 2021*a*).

Trends associated with the varying free stream velocity were subtracted from the raw time series (Hutchins *et al.*, 2012). Four 30-min records are examined in the current study and summarized in Table 1 after the following data qualifications:

1. The incoming wind direction aligned with the sensors, as verified by the sonic anemometer.
2. Near-neutral stability was reached, with both the Monin-Obukhov stability parameter $|\zeta| = |z/L| \approx 0$ and the flux Richardson number $R_f \approx 0$. The Obukhov length L is defined as

$$L = -\frac{u_*^3}{\kappa\left(g/\overline{\theta_v}\right)\overline{w'\theta_v'}}, \quad (10)$$

where g is the acceleration due to gravity, and $\overline{\theta_v}$ is the mean virtual potential temperature. The flux Richardson number R_f is defined as

$$R_f = \frac{(g/\overline{\theta_v})\overline{w'\theta_v'}}{\overline{w'u'}(d\overline{u}/dz)}. \quad (11)$$

3. Stationarity of $\overline{u}$ and turbulence intensity $u'/\overline{u}$ were observed, as assessed by the reverse arrangement test and the runs test with a 95% confidence interval (Bendat & Piersol, 2011).

LT	$\overline{u}$ (ms^{-1})	u_* (ms^{-1})	$\overline{w'\theta_v'}$ (Kms^{-1})	ζ	R_f
2000	7.55	0.28	-0.017	0.025	0.014
2030	6.56	0.22	-0.018	0.053	0.040
2200	6.60	0.24	-0.024	0.056	0.035
2230	7.34	0.29	-0.029	0.038	0.016

Table 1. Mean flow properties relative to the triaxial sonic anemometer positioned at z = 2 m for the 30-min periods analyzed (local time LT = UTC + 6 h) on 21/06/2018. The boundary layer height δ was estimated to be 60 m (Huang *et al.*, 2021*b*), and R_f was estimated using both the sonic anemometer data and the mean velocity profile given by the NSTAPs evaluated at $z = 2$ m.

The four runs satisfying these conditions were near mid-night (local time) when the stable boundary layer depth has equilibrated to its near-neutral value. Taylor's hypothesis was used to convert temporal differences in the velocity and temperature signals to spatial differences in the streamwise direction.

RESULTS

Before evaluating the model predictions, this unique dataset can be used to first assess the validity of the key assumptions underpinning the proposed model. These are (i) the tendency towards Gaussian statistics, (ii) existence of inertial range behavior, and (iii) spectral behavior consistent with the attached eddy model. The Gaussian behavior of the velocity and temperature fluctuations can be assessed using the PDFs of the measurements. The PDFs for each quantity under neutral stability conditions are shown in figure 2 at a representative measurement station corresponding to z =0.125 m. The PDFs are normalized by their standard deviation σ_u and σ_θ, respectively and their skewness $S_{u'}$ and $S_{\theta'}$ and kurtosis $K_{u'}$ and $K_{\theta'}$ are shown. The PDFs of both temperature and velocity exhibit near-Gaussian behavior, with the most evident deviations being super-Gaussian in the positive tail.

The deviations of these velocity and temperature PDFs from Gaussian behavior are highlighted in figure 3 for the same station at $z = 0.125$ m. There, each of the PDFs from figure 2 is normalized by the Gaussian distribution such that deviations from Gaussian behavior are indicated in proportion to unity. While the velocity PDF, PDF(u'/σ_u), is found to be within $\pm$10% of a Gaussian distribution for $u'/\sigma_u \leq |2|$, the scalar PDF exhibits a wider region of agreement, such that PDF(θ'/σ_θ) is within $\pm$10% for $-3 < \theta'/\sigma_\theta < 2$. However, the differences between the velocity and temperature PDFs are largest in the tails of the distribution, where deviations from Gaussian behavior are approximately twice as large for $u'/\sigma_u \geq 4$ compared to $\theta'/\sigma_\theta \geq 4$. Though the exact behavior and statistics differ with station height, the tendency for the

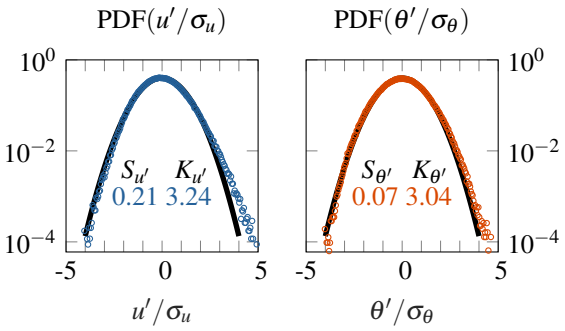

Figure 2. Measured probability density functions (open symbols) of the velocity (left) and temperature (right) fluctuations at $z = 0.125$ m. The solid black line indicates a Gaussian distribution.

temperature fluctuations towards more Gaussian behavior relative to the collocated velocity is a consistent feature across all z.

The super-Gaussian behavior in the positive tails differs from the observations of Meneveau & Marusic (2013) and Samie *et al.* (2018) who observed sub-Gaussian behavior for boundary layer measurements up to $Re_\tau = 20{,}000$, and is a potentially indicative of effects stemming from the roughness sublayer (Heisel *et al.*, 2020). Recent studies such as Marusic *et al.* (2013) and Wei *et al.* (2005) suggest that the extent of the buffer layer could be Reynolds number dependent, extending up to $z^+ \approx 3(\delta u_*/\nu)^{1/2} \approx 3 \times 10^3$, with ν being kinematic viscosity, even in smooth-wall conditions. This criteria places the lowest two measurement heights within the buffer region where sweeps tend to dominate (Heisel *et al.*, 2020), potentially explaining the observed increase in $S_{u'}$ and $K_{u'}$.

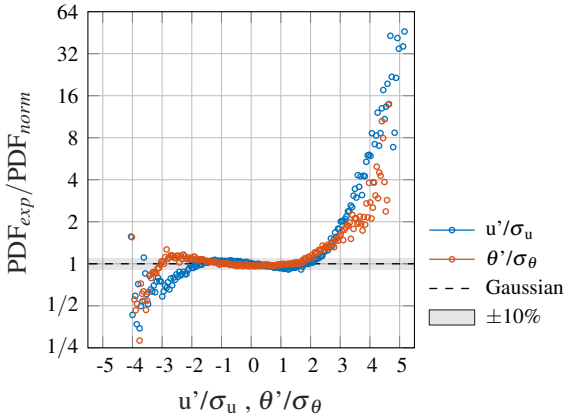

Figure 3. Deviations of measured PDFs from Gaussian behavior. PDFs of measured velocity (blue) and temperature (orange) are normalized by a Gaussian distribution given by $\mathrm{PDF}_{norm} = \exp\left(-x^2/2\right)/\sqrt{2\pi}$, where $x = u'/\sigma_u, \theta'/\sigma_\theta$. Dashed black line at unity indicates Gaussian behavior with a gray band showing the region of ±10% deviation. Values less than and greater than 1 indicate sub-Gaussian and super-Gaussian behavior, respectively.

The existence of an inertial subrange can be substantiated by assessing whether the lower order statistics of the measurements, such as mean and variance, exhibit a canonical

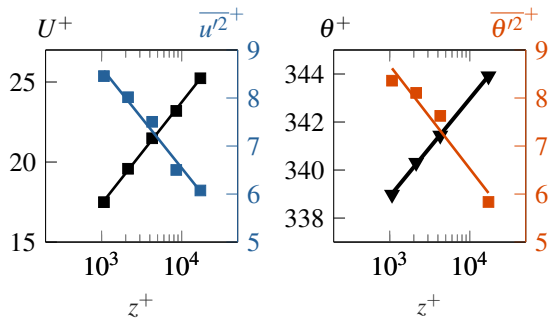

Figure 4. Mean and variance profiles for velocity (left) and temperature (right) as a function of wall distance and normalized by inner units. Mean quantities (U^+ and θ^+) are given in black, while variances for velocity ($\overline{u'^2}^+$) and temperature ($\overline{\theta'^2}^+$) are denoted in blue and orange, respectively.

logarithmic behavior. Following Vallikivi *et al.* (2015), who found logarithmic behavior above $z^+ = zu_*/\nu > 400$, the lowest measurement station to the ground at $z^+ \approx 850$ should be well within the log-layer. This assumption is further supported by the mean and variance profiles for the velocity and temperature shown in figure 4, where logarithmic behavior is found in the region $10^3 < z^+ < 10^4$. Here, $A_{1,u}$ and $A_{1,\theta}$ are estimated as 0.9 and 0.93, respectively, by a least squares fitting of the data to equation 1. This value for the velocity compares reasonably well the $A_1 \approx 1.25$ found by Meneveau & Marusic (2013).

Finally, the streamwise wavenumber spectra of the velocity and temperature fluctuations can be compared to the idealized model, each of which are shown in figure 5. In both quantities, distinct k^{-1} and $k^{-5/3}$ scaling regions are identified, consistent with the assumptions of the simplified model. However, due to the lack of convergence and stationarity of the flow, no data are available in the low wave-number region where the k^2 scaling is assumed. The expected area under the modeled k^2 region is identically equal to $\frac{1}{3}C_1$ in normalized variables. Compared to the integrated normalized spectrum of figure 5 for each case, this comes out to between 4% and 7.5% of the total integrated area. As this only affects the offset $B_{1,\theta}$ in equation 9, the overall agreement between the model spectrum and the dataset is acceptable for the purposes here.

DISCUSSION

Given the strength of the underlying assumptions and the similarity between the statistical behavior of temperature and velocity signals, the predicative capability of the proposed RSDH model in capturing the behavior of the high-order moments can be assessed. Because the temperature exhibits a distribution that more closely follows Gaussian behavior, the RSDH predictions for high-moments should hold for $(\overline{\theta'^{2p}}^+)^{1/p}$. A comparison between the high-order moments and the RSHD predictions can be seen in figure 6 for both the velocity and temperature measurements. In each case, the slope and offset of the $p = 1$ statistics (i.e., the variances) are determined from integration of the spectral RSDH models given by Katul *et al.* (2016) and the present study (see equation 7) rather than fitting a regression to the variance profiles. Similarly, the RSDH predictions for the high-order moments are determined from the $p = 1$ case through equation 9 that can be applied analogously to both velocity and temperature. Figure 6 shows that for both temperature and velocity, there appears

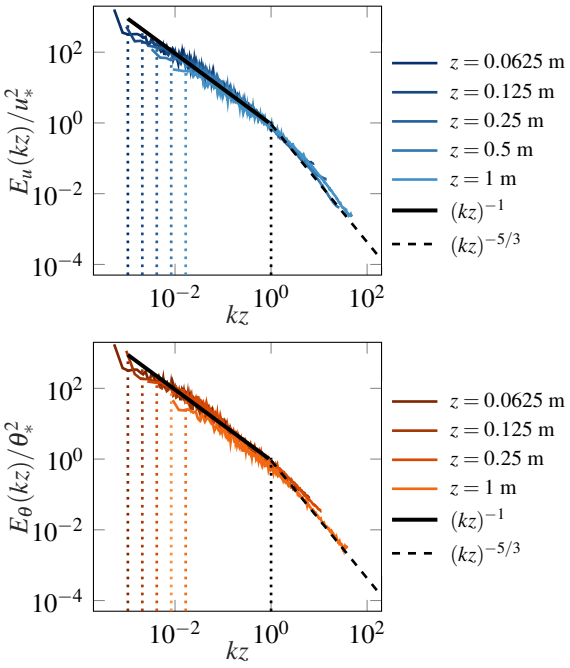

Figure 5. Normalized spectra of the longitudinal velocity ($E_u(kz)/u_*^2$) and temperature ($E_\theta(kz)/\theta_*^2$) are computed using the frozen turbulence hypothesis (Taylor, 1938) and shown as a function of normalized wavenumber kz in the upper and lower plots, respectively. Different shades of blue and orange indicate the respective spectra for velocity and temperature at the different measurement stations with lighter shades corresponding to distances further from the ground. For each quantity, there is a clear break point between the k^{-1} (——) and the $k^{-5/3}$ (– –) scaling regimes as indicated by the black vertical dotted line (···) at $k = 1/z$. The $k = 1/\delta$ cutoff between the k^2 and the k^{-1} scaling regimes are also shown for each measurement height and denoted by their respective colors noted in the legend to the right of each plot.

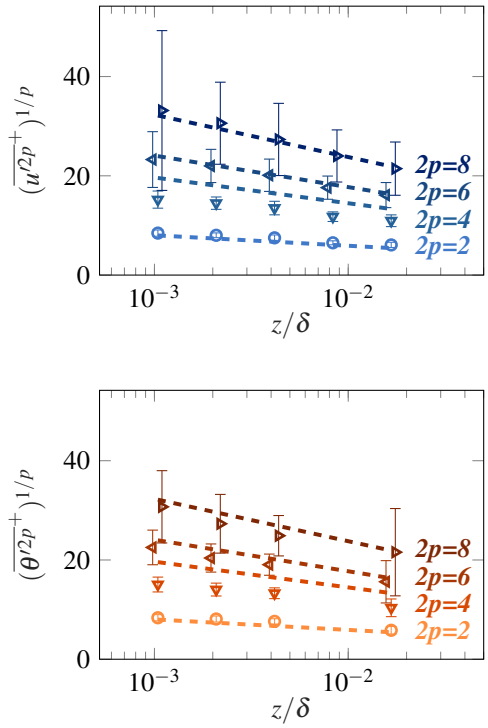

Figure 6. Profiles of high-order moments of velocity (top) and temperature (bottom) as a function of normalized distance from the ground z/δ. Central moments for $2p = 2, 4, 6$, and 8 are denoted by (○), (▽), (◁), and (▷) symbols, respectively. The dashed lines represent the predictions for high-order moments as computed using equation 1 for the velocity statistics (Katul *et al.*, 2016) and equation 9 for the temperature statistics. High-moments for velocity (blue) and temperature (orange) are denoted with darker shades of their respective colors.

to be good qualitative agreement between the measurements and their respective spectral RSDH models. In each case, the model is well within the statistical uncertainty, with the exception of the $p = 2$, partially due to the additive $(3/2)\overline{\theta'^{2p}}$ contribution as noted in the theory section of the manuscript. Further, it is difficult to discern any significant differences in the performance of the model between the two quantities.

However, the differences between the temperature and velocity statistics become more apparent in figure 7, which directly compares the slopes (A_p) and offsets (B_p) obtained from the measurements and RSDH model. There, the slope (A_p) and offset (B_p) values from the RSDH predictions are extracted from the lines shown in figure 6 and plotted in the left and right plots of figure 7, respectively, as a function of moment order p. These predictions are compared with experimental values obtained from a linear regression of the higher order moments with the logarithmic wall distance. While the performance of the RSDH model is comparable for velocity and temperature for $p \leq 3$, the agreement between the RSDH model and experimentally derived parameters is far better for temperature up to $p = 4$ than for velocity. This discrepancy is expected to widen for progressively larger values of p; however, such high-order moments are not analyzed here due to limited convergence of the statistics in the dataset.

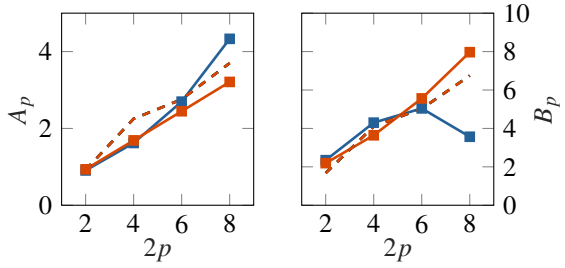

Figure 7. Coefficients A_p (blue) and $A_{p,\theta}$ (orange) as a function of moment order $2p$, averaged across available datasets. Square markers (□) denote slopes (A_p) and offsets (B_p) determined through a linear regression of the central moment profiles for $2p = 2, 4, 6$, and 8. The dashed lines represent the coefficients as predicted by integration of the spectral model and RSDH predictions given by equations 1 and 9. Due to their similarity, these RSDH predictions appear overlapping.

CONCLUSIONS

The similarity between temperature and momentum is used to propose a new theory for the behavior of passive scalar moments in the inertial sublayer based on RSDH. The predicted behavior from the new model is found to be in good agreement with highly resolved measurements of temperature obtained in the atmospheric surface layer under near-neutral conditions with deviations significantly smaller from RSDH

behavior than their collocated streamwise velocity counterpart. While the performance of the new model is encouraging, extending and evaluating this framework under non-neutral stability conditions and turbulent $Pr \neq 1$ remains an area of future investigation.

REFERENCES

Arwatz, Gilad, Fan, Yuyang, Bahri, Carla & Hultmark, Marcus 2015 Development and characterization of a nanoscale temperature sensor (T-NSTAP) for turbulent temperature measurements. *Measurement Science and Technology* **26** (3), 035103.

Bendat, Julius S & Piersol, Allan G 2011 *Random data: analysis and measurement procedures*. John Wiley & Sons.

Heisel, Michael, Katul, Gabriel G, Chamecki, Marcelo & Guala, Michele 2020 Velocity asymmetry and turbulent transport closure in smooth-and rough-wall boundary layers. *Physical Review Fluids* **5** (10), 104605.

Huang, K Y, Brunner, C E, Fu, M K, Kokmanian, K, Morrison, T J, Perelet, A O, Calaf, M, Pardyjak, E & Hultmark, M 2021*a* Investigation of the atmospheric surface layer using a novel high-resolution sensor array. *Experiments in Fluids* **62** (4), 1–13.

Huang, Kelly Y. & Katul, Gabriel G. 2022 Profiles of high-order moments of longitudinal velocity explained by the random sweeping decorrelation hypothesis. *Physical Review Fluids* **7** (4), 044603.

Huang, Kelly Y, Katul, Gabriel G & Hultmark, Marcus 2021*b* Velocity and temperature dissimilarity in the surface layer uncovered by the telegraph approximation. *Boundary-Layer Meteorology* pp. 1–21.

Hultmark, Marcus, Ashok, Anand & Smits, Alexander J. 2011 A new criterion for end-conduction effects in hot-wire anemometry. *Measurement Science and Technology* **22** (5), 055401.

Hutchins, Nicholas, Chauhan, Kapil, Marusic, Ivan, Monty, Jason & Klewicki, Joseph 2012 Towards reconciling the large-scale structure of turbulent boundary layers in the atmosphere and laboratory. *Boundary-layer meteorology* **145** (2), 273–306.

Katul, Gabriel G, Banerjee, Tirtha, Cava, Daniela, Germano, Massimo & Porporato, Amilcare 2016 Generalized logarithmic scaling for high-order moments of the longitudinal velocity component explained by the random sweeping decorrelation hypothesis. *Physics of Fluids* **28** (9), 095104.

Katul, Gabriel G, Chu, Chia R, Parlange, Marc B, Albertson, John D & Ortenburger, Teresa A 1995 Low-wavenumber spectral characteristics of velocity and temperature in the atmospheric surface layer. *Journal of Geophysical Research: Atmospheres* **100** (D7), 14243–14255.

Klewicki, J C, Foss, J F & Wallace, J M 1998 High Reynolds number [R_θ= O(10^6)] boundary layer turbulence in the atmospheric surface layer above western Utah's salt flats. In *Flow at Ultra-High Reynolds and Rayleigh Numbers*, pp. 450–466. Springer.

Li, Dan, Katul, Gabriel George & Gentine, Pierre 2016 The k-1 scaling of air temperature spectra in atmospheric surface layer flows. *Quarterly Journal of the Royal Meteorological Society* **142** (694), 496–505.

Marusic, I., Monty, J.P., Hultmark, M. & Smits, A.J. 2013 On the logarithmic region in wall turbulence. *J. Fluid Mech.* **716**, R3.

Meneveau, Charles & Marusic, Ivan 2013 Generalized logarithmic law for high-order moments in turbulent boundary layers. *Journal of Fluid Mechanics* **719**, R1.

Metzger, M M & Klewicki, J C 2001 A comparative study of near-wall turbulence in high and low Reynolds number boundary layers. *Physics of Fluids* **13** (3), 692–701.

Morrison, T, Calaf, M, Higgins, C, Drake, S.A., Perelet, A. & Pardyjak, E. 2021 The impact of surface temperature heterogeneity on near-surface heat transport. *Boundary-Layer Meteorology* .

Pirozzoli, Sergio, Bernardini, Matteo & Orlandi, Paolo 2016 Passive scalars in turbulent channel flow at high reynolds number. *Journal of Fluid Mechanics* **788**, 614–639.

Pond, S, Smith, SD, Hamblin, PF & Burling, RW 1966 Spectra of velocity and temperature fluctuations in the atmospheric boundary layer over the sea. *Journal of Atmospheric Sciences* **23** (4), 376–386.

Samie, M, Marusic, I, Hutchins, N, Fu, M K, Fan, Y, Hultmark, M & Smits, A J 2018 Fully resolved measurements of turbulent boundary layer flows up to Re_τ = 20,000. *Journal of Fluid Mechanics* **851**, 391–415.

Smits, Alexander J., McKeon, Beverley J. & Marusic, Ivan 2011 High–Reynolds Number Wall Turbulence. *Annual Review of Fluid Mechanics* **43** (1), 353–375.

Taylor, Geoffrey Ingram 1938 The spectrum of turbulence. *Proceedings of the Royal Society of London. Series A-Mathematical and Physical Sciences* **164** (919), 476–490.

Tennekes, H 1975 Eulerian and lagrangian time microscales in isotropic turbulence. *Journal of Fluid Mechanics* **67** (3), 561–567.

Vallikivi, M., Hultmark, M. & Smits, A. J. 2015 Turbulent boundary layer statistics at very high Reynolds number. *Journal of Fluid Mechanics* **779**, 371–389.

Wei, T, Fife, P, Klewicki, J & McMurtry, P 2005 Properties of the mean momentum balance in turbulent boundary layer, pipe and channel flows. *Journal of Fluid Mechanics* **522**, 303–327.

Yeung, P. K. & Sawford, Brian L. 2002 Random-sweeping hypothesis for passive scalars in isotropic turbulence. *Journal of Fluid Mechanics* **459**, 129–138.